Multiphoton Dissociation of Electrosprayed MegaDalton-Sized DNA Ions in a Charge-Detection Mass Spectrometer

ARTICLE *in* JOURNAL OF THE AMERICAN SOCIETY FOR MASS SPECTROMETRY · OCTOBER 2014

Impact Factor: 2.95 · DOI: 10.1007/s13361-014-1011-z · Source: PubMed

J. Am. Soc. Mass Spectrom. (2015) 26:7–13
DOI: 10.1007/s13361-014-1011-z

RESEARCH ARTICLE

Multiphoton Dissociation of Electrosprayed MegaDalton-Sized DNA Ions in a Charge-Detection Mass Spectrometer

Tristan Doussineau,[1,2] Pierre Paletto,[1,2] Philippe Dugourd,[1,2] Rodolphe Antoine[1,2]

[1]Université Claude Bernard Lyon1-CNRS, Université de Lyon, 69622 Villeurbanne cedex, France
[2]Institut lumière matière, UMR5306, Villeurbanne, France

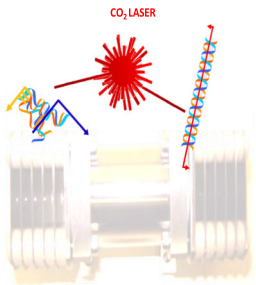

Abstract. Charge detection mass spectrometry in combination with a linear electrostatic ion trap coupled to a continuous wavelength infrared CO^2 laser has been used to study the multiphoton dissociation of DNA macromolecular ions. Samples, with masses ranging from 2.23 to 31.5 MDa, include single strand circular M13mp18, double strand circular M13mp18, and double strand linear LambdaPhage DNA fragments. Their activation energies for unimolecular dissociation were determined. Activation energy values slightly increase as a function of the molecular weight. The most important result is the difference between the fragmentations observed for hybridized double-strands and dimers of single strands.

Keywords: Charge detection mass-spectrometry, Single-molecule, Oligonucleotide, Gas-phase, Radiative dissociation, Electrospray ions, Nucleic-acids, Activation, Charge

Received: 12 May 2014/Revised: 17 September 2014/Accepted: 20 September 2014/Published online: 28 October 2014

Introduction

Mass spectrometry (MS)-based techniques have initiated active developments in the analysis of nucleic acids, fueled by methods based on electrospray (ESI) and matrix-assisted laser desorption ionization (MALDI). For selected applications in genomics, mass spectrometry is now competitive with other analytical techniques [1, 2] such as capillary gel electrophoresis (CE) and laser-induced fluorescence in particular for applications focused on the characterization of single nucleotide polymorphisms (SNPs) and short tandem repeats (STRs) [3, 4]. However, because of its comparably low read length [<100 nucleotides (nts) for MS versus <1000 nts for CE], MS is not capable of substituting CE.

The study of macromolecules and macromolecular complexes by MS is further complicated because of ion heterogeneity, a problem that can be solved by detection of individual ions. Recent years have seen significant advances in the characterization and manipulation of individual molecules. For instance, the combination of single-DNA molecule fluorescence and micromanipulation has provided a new method for testing polymer dynamics and DNA–protein interactions [5, 6]. On the other hand, new techniques that monitor ionic current modulations as single molecules pass through a nanoscale pore have enabled numerous single-molecule studies [7], and is used for example for discrimination between classes of nucleic acids, or detection of DNA binding [8]. Detection of individual megadalton DNA ions by mass spectrometry was pioneered by Smith and coworkers using a Fourier transform ion cyclotron resonance (FT-ICR) mass spectrometer [9, 10] and by Benner and coworkers using a charge-detection (CD) electrostatic ion trap [11]. Thanks to the trapping capability of these MS devices, individual plasmid DNA ions in the megadalton range were detected and measured with an accuracy of approximately 10%.

Sequence confirmation and de novo sequence determination, as well as characterization of the intrinsic forces governing structure and function are generally achieved through tandem MS [12–15]. Infrared multiphoton dissociation (IRMPD) is particularly efficient for DNA, either by absorption of IR photons from black-body radiation or after CO_2 laser excitation, because of the phosphate moiety located along their backbone structure, which yields excellent photon absorption at $\lambda = 10.6$ μm [16, 17]. The strength of the glycosidic bond [18], and also of the Watson-Crick or other hydrogen-bonding

Electronic supplementary material The online version of this article (doi:10.1007/s13361-014-1011-z) contains supplementary material, which is available to authorized users.

Correspondence to: Rodolphe Antoine; *e-mail:* rodolphe.antoine@univ-lyon1.fr

interactions that hold together the oligonucleotide chains, has been probed by IRMPD experiments [19]. Tandem MS, however, is usually limited to elucidation of the sequence of small oligonucleotides (<20 nts).

We recently pushed to the megadalton range the boundary of photofragmentation experiments utilizing infrared multiphoton dissociation on single macroions, using a charge detection electrostatic trap coupled to a CO_2 laser [20, 21]. In particular, our experimental approach extracts activation energies for dissociation and reveals several fragmentation pathways having distinct signatures at the single-molecule level that would not be accessible from studies based on statistically averaged reaction rates only [22]. Here, we report the use of infrared multiphoton dissociation (IRMPD) for the determination of relative activation energies for unimolecular dissociation of double-strand and single-strand megadalton-sized DNA electrospray ions. The aim of this study is to establish a relationship between both activation energies and dissociation patterns and the molecular structure, in particular hydrogen-bonding interactions of DNAs.

Experimental

Chemicals

Lambda DNA mixed digest was supplied from Sigma-Aldrich (Saint-Quentin Fallavier, France). The digest sample contains 10 fragments ranging from 1053 to 48502 bp (from 0.7 to 31.5 MDa). M13mp18 RF I DNA and M13mp18 DNA were supplied by New England Biolabs (Evry, France). M13mp18 RF I DNA is the double-strand, covalently closed, circular form of DNA derived from bacteriophage M13. Lambda DNA mixed digest, M13mp18 RF I DNA, and M13mp18 single-stranded DNA samples were provided in buffered aqueous solution of 10 mM Tris–HCl with 1 mM ethylenediaminetetraacetic acid. Sampling operation before injection in electrospray ionization source typically consists of diluting DNA in a water:acetonitrile = 1:3 solvent mixture to a concentration of 0.01 g/L.

Infrared Multiphoton Dissociation Charge Detection Mass Spectrometry

Experiments were performed on an electrostatic ion trap of the type used by Benner [11] coupled to an electrospray ionization source and a continuous CO_2 laser, as described recently [20–22]. Gas-phase ions generated in positive mode electrospray were transmitted through a hexapole and ionic lenses and directed toward the charge detection chamber. When an ion enters the charge detection device (CDD), it triggers a circuit that places the potentials on the entrance and exit electrodes (ion mirrors) to predetermined values chosen to reflect ions. Trapping potentials are applied for as long as 42 ms. With the current setup, the noise level in the pick-up signal is ~400 e (e = 1.602 10^{-19} C). Fragment ions with total charges lower than 400 e cannot be detected. During the trapping time, the ions can be fragmented by exposure to CO_2 laser (cw laser at λ = 10.6 μm, output maximum power of 25 W, beam diameter of 8.1 mm in the trap). The laser beam is reflected by two gold-coated copper mirrors, after which it is aimed along the axis of the ion trap through a ZnSe window fitted on the rear of the CDD chamber. For laser power dependency experiments, the laser output was chopped electronically with a 5 kHz pulse train chosen to realize duty cycles between 10% and 99%.

Sets of 5-hundreds individual raw time domain signal are recorded at each laser power as well as without laser irradiation (as a blank). Each wavelet that has trapping time longer than 2 ms is individually processed. The processing includes the determination of the average signals amplitude and the average time-of-flight $\langle \Delta t \rangle$ of the ions. Average amplitude is translated to a charge number z using a calibration test capacitor that allowed a known amount of charge to be pulsed onto the pick-up tube. The calibration test pulses were generated with a shaping-pulse generator so that the time-dependent signal response could be determined as well. The mass-to-charge ratio m/z of an ion is determined from the average time-of-flight $\langle \Delta t \rangle$ through the tube. The ion velocity v_m is equal to $L/\langle \Delta t \rangle$, where L is the length of the detector tube (i.e., 3.75 cm). Then it becomes Equation 1: [23]

$$\frac{m}{z} = \frac{2eV}{v_m^2 - v_g^2} \tag{1}$$

where m is the mass, z is the number of charges of the ions, and V the electrostatic acceleration voltage. In our system, a correction is needed to take into account the initial kinetic energy imparted to the ion by the free jet expansion of the gas prior to acceleration by the electric field. To do so, v_g, the ion velocity attributable to the free gas expansion, is measured. It is determined by grounding all electrostatic lenses and timing the passage of the ion through the detector. These procedures allow us to internally calibrate our charge detection mass spectrometer. Finally, in charge detection mass spectrometry, the mass m is calculated using Equation 2:

$$m = \frac{2zeV}{v_m^2 - v_g^2} \tag{2}$$

Furthermore, both onset time (time at which fragmentation starts), and disappearance time (time beyond which an ion fragment is no longer detected) are extracted from each trapped ion signal. Charge decay patterns are also individually analyzed according to their shape. If time duration between onset time and disappearance time does not exceed 200 μs (or three oscillations of any detected ion fragment within the trap), the charge decay profile is classified as "sudden loss." If this fragmentation duration exceeds 200 μs, decay shapes are then classified in two different categories (vide supra): (1) decay shapes named "funnel" are assigned to those that progressively lose charges until disappearance; (2) "staircase"-type decays correspond to a sudden loss of a certain amount of charges from the parent ion, leading to a stable fragment that stays as produced within the trap longer than 200 μs (or three

oscillations). Also "hybrid"-type decays that mix both above mentioned shapes are observed, but infrequently.

Results and Discussion

Mass and Charge Data

Positive ion CD mass spectra of single-stranded M13mp18 and double strand M13mp18 RF I DNA samples are plotted in Figure 1. These plots represent the measurement of about 1500 individual trapped ions. Mass and charge were individually extracted from each transient waveform as described in Experiment section.

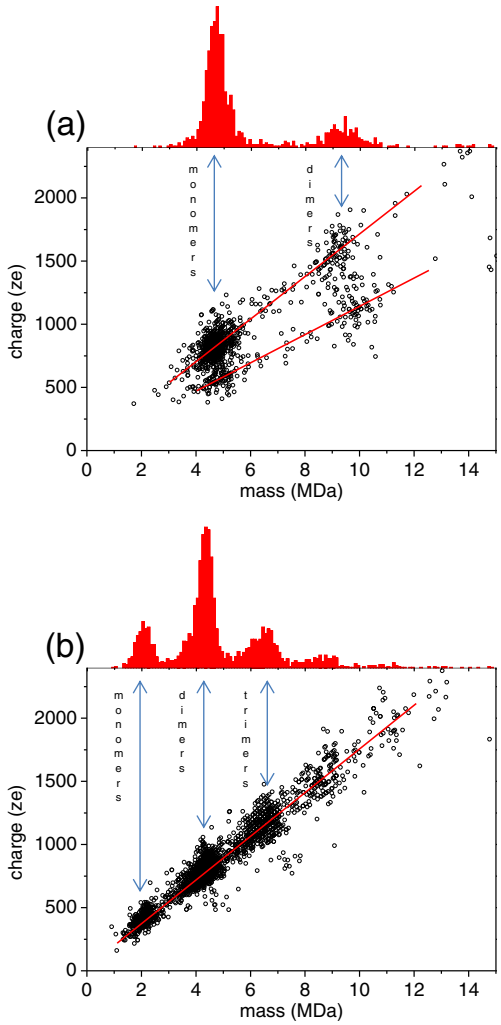

Figure 1. CD-MS scatter plots of charge versus mass for **(a)** double strand M13mp18 RF I, and **(b)** single-stranded M13mp18 DNA samples. Each point corresponds to an individual measurement. Each spot can be assigned to an aggregation state of the ds DNA (i.e., monomer, dimer, and trimer). Projection of the scatter plots on the mass axis provides the corresponding mass histograms (bin size = 0.1 MDa). Solid red lines are representative of the charge states (i.e., m/z = 5800 and m/z = 8700 for ds M13mp18 RF I, and m/z = 5800 for single-stranded M13mp18, respectively)

Figure 1a displays four clusters of data points attributed to monomer and dimer of double strand M13mp18 RF I. The measured average mass for double strand M13mp18 RF I deviates of about 5% from the nominal mass value ($\langle m_{measured} \rangle$ = 4.71 MDa compared with $\langle m_{nominal} \rangle$ = 4.48 MDa). The width of the peaks in the histogram of RF I M13mp18 M13mp18 (Figure 1a) corresponds to $m/\Delta m \sim 6$ for the monomer and $m/\Delta m \sim 7$ for the dimer species (Δm = FWHM of the fitted mass peak). The values are lower than the expected ones (i.e., $m/\Delta m \sim 10$ for the monomer and $m/\Delta m \sim 17$ for the dimer species, more details about resolution of the CDMS apparatus are given in Supporting Materials) and may be attributed to the fact that the samples were poorly desalted. The observed broadening may be caused by different amounts of residual salt adduction and, to a lesser extent, solvent molecules added in the gas phase [24]. There are two different charge states for ions with a mass corresponding to RF I M13mp18, one centered at 810 e (m/z ~5800) and the other at 580 e (m/z ~8700). These two charge states could reflect that ions are present in solution in two different conformations, each leading to a different charge state as already mentioned in previous studies by Benner and coworkers on megadalton-DNA electrospray ions using charge detection mass spectrometry [24, 25]. Similar m/z distributions are observed for dimers.

In Figure 1b, several spots positioned on the linear function m/z ~5800 are observed and attributed to DNA oligomers. Peaks assigned to the unfragmented ss/circular M13mp18 and its dimeric and trimeric forms are highlighted in Figure 1b. The peaks are slightly skewed to lower MWs, presumably because of fragmented DNA [25]. The mass values obtained for ds/circular and ss/circular DNA samples are collected in Table 1 as well as those from ds/linear samples. In general, precision on the measured masses by CD-MS is good with deviation never exceeding ±5% compared with nominal mass values. For larger DNA, in addition to sodium and solvent adduction, the possible presence of oligomeric DNAs (noncovalent multimers of nucleic acids) might broaden the distribution towards higher masses. Another possible source of higher mass species is concatemer formation of the high copy number plasmid in vivo [26]. Representative positive ion CD mass spectra of LambdaPhage DNA mixed digest are depicted in Figure 2. Resolved peaks can be observed by projecting the scatter plots on the mass axis providing the corresponding mass spectrum of LambdaPhage DNA Mixed Digest (see Figure 2). Interestingly, 11.0 MDa ds/linear Lambda DNA exhibits a mass-to-charge ratio of 9500, whereas heavier studied samples (i.e., 18.5 and 30.0 MDa), have mass-to-charge ratios of 17,100 and 16,500, respectively. This may suggest that there is a transition in the conformation of the ions as their size increases, from an extended conformation at smaller size to a more compact one at bigger size. The charging capacity of compact structures is lower than the one of extended structures because of the smaller accessible surface. For circular DNA samples, the m/z values are similar for different oligomers (i.e., 5800). This may indicate that the charging capacity of DNA ions is mainly driven by the charging capacity of the monomer unit.

Table 1. Features of Studied DNA and Corresponding Combined CD-MS/IRMPD Data

DNA denomination	Features	Aggregation state	$\langle m_{nominal} \rangle$ [a]	$\langle m_{measured} \rangle$	m/z	E_a	t_o [c]	$t_{1/2}$ [c]
			(MDa)	(MDa)	(Th)	(eV)	(ms)	(ms)
LambdaPhage	ds/linear/ 48502 bp	monomer	31.5	30.0	16500	0.36 ± 0.05[b]	18.0	19.5
		monomer	19.4	18.5	17100	0.31 ± 0.05	15.5	17.2
		monomer	11.1	11.0	9000	0.20 ± 0.05	8.9	14.0
M13mp18 RF I	ds/circular/ 7249 bp	monomer	4.48	4.70	5800	0.20 ± 0.07	6.7	8.9
M13mp18, single-stranded	ss/circular/ 7249 bp	monomer	2.24	2.09	5800	0.14 ± 0.07	5.9	6.8
		dimer	4.48	4.33	5800	0.13 ± 0.07	5.9	6.6
		trimer	6.72	6.42	5800	0.20 ± 0.07	5.8	6.5

[a] Calculated using the known DNA sequence.
[b] Taken from Reference [21].
[c] At laser power of 6.4 W/cm^2. t_o: onset time *and* $t_{1/2}$: half lifetime

Activation Energies for Dissociation

In the ion trap, single trapped ions undergo several hundred round trips between the ion mirrors. The corresponding image current generated by the round trips of ions in the trap (oscillations) is then recorded as a function of time. As the laser is switched on during the ion trapping time, drastic changes are observed in the trapping times. As shown in Figure 3, under continuous irradiation by the CO_2 laser (6.4 W/cm^2), the ion has a trapping time that does not exceed 10 ms.

Our approach for interpreting the observed kinetics for the dissociation of DNA electrospray ions consisted of analyzing a large set of wavelets of individual ions in order to construct a frequency histogram of the distribution of dissociation rates for a collection of ions. Individual trapped ions were irradiated for 42 ms with a laser output power ranging from 10% to 99% [21]. For each laser power, ~100 wavelets of individual ions were analyzed. The normalized ion count at a given time was obtained by the number of traces for which the ion was still detected at this time and by normalization over the initial number of traces that was considered. An onset time of fragmentation is required to heat the ions from room temperature until they are hot enough for dissociation to start. This onset time decreases with laser intensity. After the onset time, ion dissociation produces an exponential decrease in parent ion count (straight lines in Figure 4a, b). Here the kinetics is measured after the onset time. The rate of dissociation increases with laser intensity (see Figure 4c) and can be evaluated for each laser power from the linear fit using $k_{diss} = -d\ ln(C_I)/dt$, where C_I is the ion count. By acquiring the first-order rate constants at different laser intensities (see Figure 4c), plotting of the natural logarithm of the rate constant versus the natural logarithm of the laser intensity yields an activation energy E_a for the photodissociation process according to the Equation 3: [21, 27]

$$E_a = 0.22 \frac{d\ln k_{diss}}{d\ln \rho(\nu_{laser})} \quad (3)$$

The activation energy values obtained for the studied DNA samples are collected in Table 1.

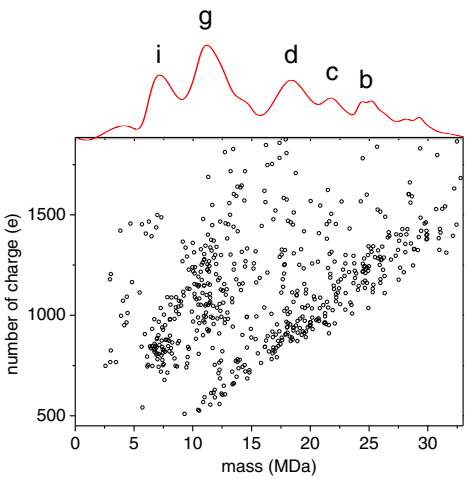

fragment	bp	mass (MDa)
a	48502	31,5
b	38416	24,9
c	33498	21,7
d	29946	19,4
e	24508	15,9
f	23994	15,6
g	17053	11,1
h	15004	9,7
i	10086	6,9
j	1053	0,69

Figure 2. CD-MS scatter plots of charge versus mass for LambdaPhage DNA mixed digest (bottom left). Projection of the scatter plots on the mass axis provides the corresponding mass spectrum (bin size = 0.5 MDa, and additional smoothing of data). Table of base pair number (bp) and mass of the 10 fragments constituting the digest (right). Tentative assignment of fragments is reported on the mass spectrum

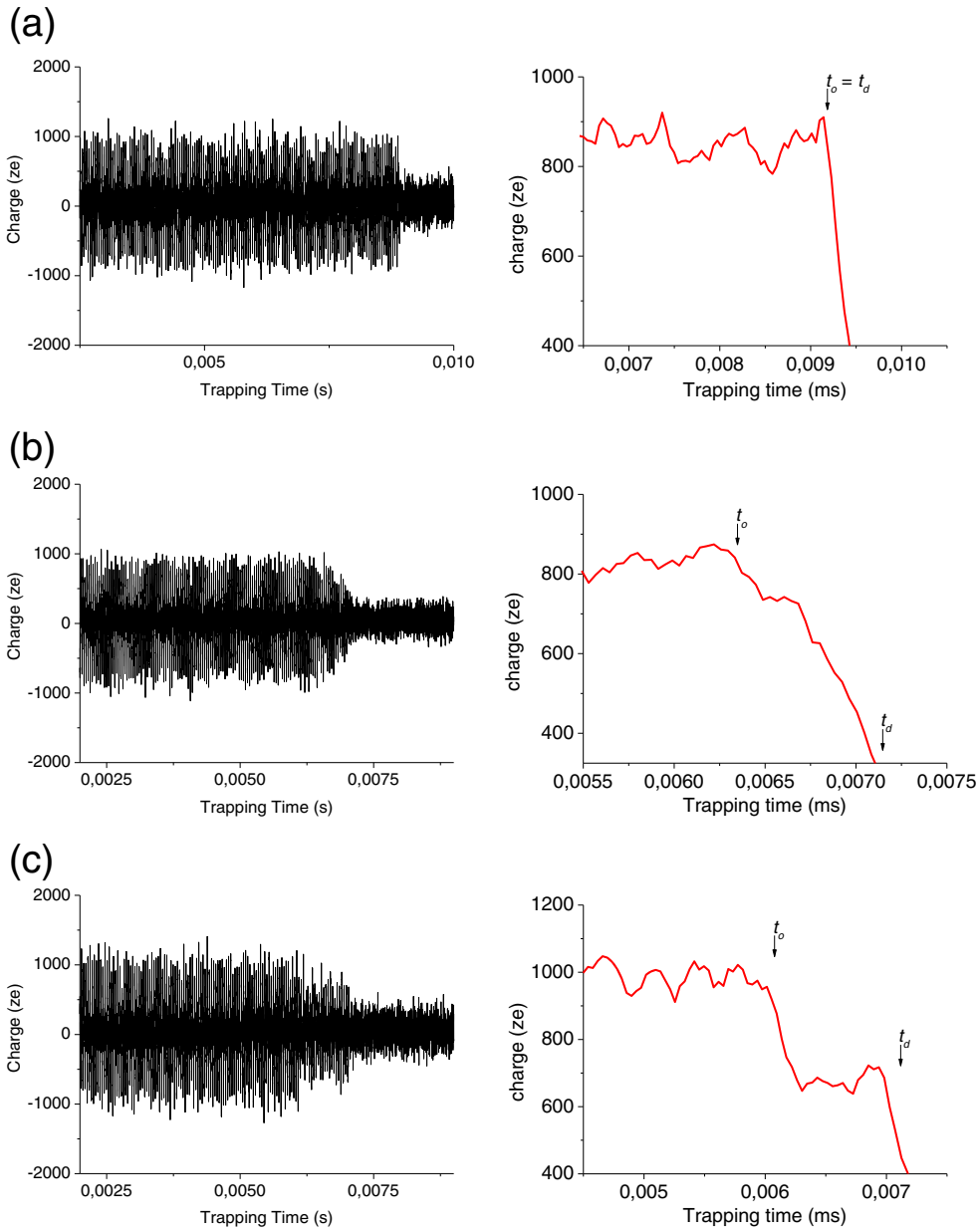

Figure 3. (Left) Waveforms of a single trapped ds/circular M13mp18 electrosprayed ion at 6.4 W/cm^2 laser irradiation highlighting **(a)** "sudden-loss," **(b)** "funnel," and **(c)** "staircase" types of decay shape. (Right) The red curve shows the evolution of the total number of elementary charges of trapped ions as a function of time. A smoothing of raw data using adjacent averaging (10 points) has been used. Onset time (t_o) and disappearance time (t_d) are also indicated for each waveform

(i) E_a values slightly increase as a function of the molecular weight, as exemplified with LambdaPhage DNA and two of its digests. A good correlation coefficient of 0.96 is found between activation energies and onset times. In other words, more important is the activation energy, longer is the heating time. A similar correlation is found between half lifetime (time at which half of the ion population has disappeared) and activation energies (see Table I). (ii) The hybridized ds M13mp18 DNA has a slightly higher activation energy (i.e., 0.20 ± 0.07 eV) than the non-hybridized dimer of ss M13mp18 (i.e., 0.13 ± 0.07 eV). This may be correlated with the base pairing in the hybridized strands, which is stronger than in non-hybridized ones.

Multiphoton Dissociation of DNA Electrospray Ions at the Single-Molecule Level

As already observed for polymer macroions [22], the waveforms recorded under laser irradiation reveal several fragmentation pathways having distinct signatures at the single-molecule level. Three types of fragmentation patterns have been observed. The traces display, in addition to "sudden loss" type, "funnel" type

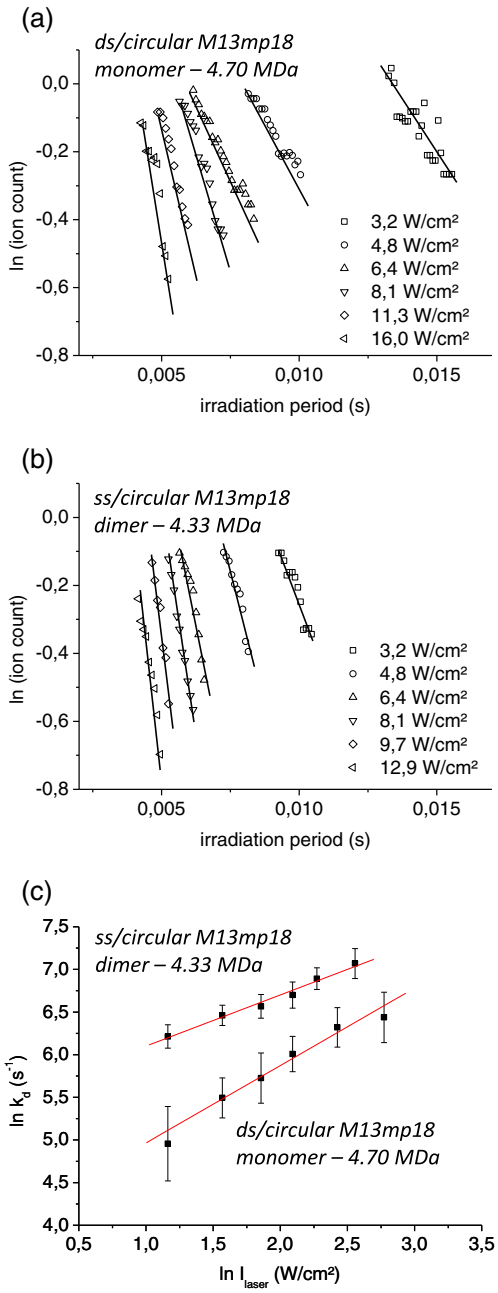

Figure 4. Logarithm of ion count versus time for the dissociation of **(a)** ds/circular M13mp18 DNA in its monomeric aggregation state, and **(b)** ss/circular M13mp18 DNA in its dimeric aggregation state under different laser power irradiation. The plots were constructed by analyzing ~100 wavelets of individual ions at each laser power in order to construct a frequency histogram of the distribution of ion counts. The line corresponds to a linear fit of the data. **(c)** Respective plots of the logarithm of the first-order unimolecular dissociation rate constant, k_{diss}, versus the logarithm of the laser intensity for both DNA samples. The activation energy for dissociation, E_a, is obtained from the slope of the linear fit (see Equation 3)

and "staircase" type behaviors (see Figure 3) [22]. The individual traces provide the opportunity to compare the repartition in the shape of the decay wavelets for DNA ions. As an example,

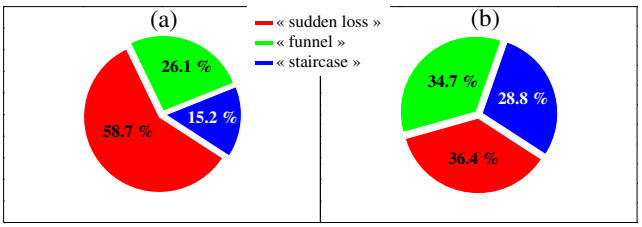

Figure 5. Repartition in shape of the decay wavelets for hybridized ds M13mp18 RF I DNA **(a)**, and non-hybridized dimer of ss M13mp18 **(b)** at 6.4 W/cm^2 CO_2 laser irradiation

Figure 5 displays the repartition in the shape of the decay wavelets for hybridized ds M13mp18 DNA and non-hybridized dimer of ss M13mp18. The proportions of the different type of traces do not significantly depend on the laser power. The "sudden loss" percentage is significantly reduced in the case of non-hybridized dimer of ss M13mp18 (Figure 5b) compared with the one reported for the hybridized ds M13mp18 RF I DNA (Figure 5a). The "sudden loss" events are attributed to multiphoton dissociation resulting in fragment ions that are not stored in the ion trap. Strand separation is included in the latter category. The formation of fragments at half the mass of the parent leads to a charge state around ~350 e, which is lower than our detection limit. On the other hand, for non-hybridized species, the fragmentation patterns display an increase in the "funnel" and "staircase" events. For non-hybridized species, the two strands are not fully base-paired compared with the ds M13mp18 RF I DNA (vide supra). The fragmentation patterns show that fragmentation is not dominated by strand separation but by partial fragmentation, which may follow partial unzipping of the two strands. The lower average charge state observed for this system compared with ds M13mp18 RF I DNA and the fragmentation pattern suggest two monomers bound by a complex hydrogen bond network leading to compact structure with a low surface area. Activation energies reflect a higher stability for double-strand monomer than for single-strand dimer, the latter being subject to easier partial fragmentation. For non-hybridized species, the difficulty of separating the two strands compared with partial fragmentation may reflect topological constraints. Once started, it is easier to unzip an organized structure than an entangled one, as observed for macroscopic zippers or for plectonemically supercoiled DNA structures [28, 29].

Conclusion

We reported the use of a continuous-wave (cw) CO_2 laser for the determination of activation energy for unimolecular dissociation of megadalton DNA ions. Single megadalton DNA ions were trapped and irradiated with the laser. The analysis of wavelets as a function of time allowed us to extract the dissociation rate constant for several laser intensities. A plot of the logarithm of the first-order rate constant versus the logarithm of laser intensity yields a straight line, the slope of which provides a measure of the activation energy for dissociation. Activation

energy values slightly increase as a function of the molecular weight. A good correlation (correlation coefficient 0.95) between activation energies and times for dissociation (both onset time and half lifetime) is found. Interestingly, hybridized versus non-hybridized structures can be discriminated by their activation energy.

The experiment reveals several fragmentation pathways having distinct signatures at the single molecule level, which would not be accessible from studies based on statistically averaged reaction rates only. However, the sensitivity of our CDMS instrument has to be improved in order to fully detect low-mass fragments for a complete exploration of multiphoton dissociation patterns of DNA ions. Works in these lines are currently being undertaken by our group.

Acknowledgments

The authors gratefully acknowledge the ANR for financial support of this work (grants no. ANR-08 BLAN-0110-01 and no. ANR-11-PDOC-032-01). The authors thank Xavier Dagany, Christian Clavier, Michel Kerleroux, Marc Barbaire, Jacques Maurelli, and Congyu Bao for their invaluable assistance.

References

1. Huber, C.G., Oberacher, H.: Analysis of nucleic acids by on-line liquid chromatography-mass spectrometry. Mass Spectrom. Rev. **20**, 310–343 (2001)
2. Oberacher, H.: On the use of different mass spectrometric techniques for characterization of sequence variability in genomic DNA. Anal. Bioanal. Chem. **391**, 135–149 (2008)
3. Seichter, D., Krebs, S., Förster, M.: Rapid and accurate characterisation of short tandem repeats by MALDI-TOF analysis of endonuclease cleaved RNA transcripts. Nucleic Acids Res. **32**, e16 (2004)
4. Hannis, J.C., Muddiman, D.C.: Genotyping short tandem repeats using flow injection and electrospray ionization Fourier transform ion cyclotron resonance mass spectrometry. Rapid Commun. Mass Spectrom. **15**, 348–350 (2001)
5. Mehta, A.D., Rief, M., Spudich, J.A., Smith, D.A., Simmons, R.M.: Single-molecule biomechanics with optical methods. Science **283**, 1689–1695 (1999)
6. Saleh, O.A., Allemand, J.-F., Croquette, V., Bensimon, D.: Single-molecule manipulation measurements of DNA transport proteins. Chem. Phys. Chem. **6**, 813–818 (2005)
7. Howorka, S., Siwy, Z.L.: Nanopore analytics: sensing of single molecules. Chem. Soc. Rev. **38**, 2360–2384 (2009)
8. Branton, D., Deamer, D.W., Marziali, A., Bayley, H., Benner, S.A., Butler, T., Di Ventra, M., Garaj, S., Hibbs, A., Huang, X.H., Jovanovich, S.B., Krstic, P.S., Lindsay, S., Ling, X.S.S., Mastrangelo, C.H., Meller, A., Oliver, J.S., Pershin, Y.V., Ramsey, J.M., Riehn, R., Soni, G.V., Tabard-Cossa, V., Wanunu, M., Wiggin, M., Schloss, J.A.: The potential and challenges of nanopore sequencing. Nat. Biotechnol. **26**, 1146–1153 (2008)
9. Bruce, J.E., Cheng, X., Bakhtiar, R., Wu, Q., Hofstadler, S.A., Anderson, G.A., Smith, R.D.: Trapping, detection, and mass measurement of individual ions in a Fourier-transform ion-cyclotron resonance mass spectrometer. J. Am. Chem. Soc. **116**, 7839–7847 (1994)
10. Smith, R.D., Cheng, X., Bruce, J.E., Hofstadler, S.A., Anderson, G.A.: Trapping, detection, and reaction of very large single molecular-ions by mass-spectrometry. Nature **369**, 137–139 (1994)
11. Benner, W.H.: A gated electrostatic ion trap to repetitiously measure the charge and *m/z* of large electrospray ions. Anal. Chem. **69**, 4162–4168 (1997)
12. Wu, J., McLuckey, S.A.: Gas-phase fragmentation of oligonucleotide ions. Int. J. Mass Spectrom. **237**, 197–241 (2004)
13. McLuckey, S.A., Vanberkel, G.J., Glish, G.L.: Tandem mass spectrometry of small, multiply charged oligonucleotides. J. Am. Soc. Mass Spectrom. **3**, 60–70 (1992)
14. Oberacher, H., Mayr, B.M., Huber, C.G.: Automated de novo sequencing of nucleic acids by liquid chromatography-tandem mass spectrometry. J. Am. Soc. Mass Spectrom. **15**, 32–42 (2004)
15. Murray, K.K.: DNA sequencing by mass spectrometry. J. Mass Spectrom. **31**, 1203–1215 (1996)
16. Brodbelt, J.S., Wilson, J.J.: Infrared multiphoton dissociation in quadrupole ion traps. Mass Spectrom. Rev. **28**, 390–424 (2009)
17. Dunbar, R.C.: BIRD (blackbody infrared radiative dissociation): evolution, principles, and applications. Mass Spectrom. Rev. **23**, 127–158 (2004)
18. Klassen, J., Schnier, P., Williams, E.: Blackbody infrared radiative dissociation of oligonucleotide anions. J. Am. Soc. Mass Spectrom. **9**, 1117–1124 (1998)
19. Schnier, P.D., Klassen, J.S., Strittmatter, E.E., Williams, E.R.: Activation energies for dissociation of double strand oligonucleotide anions: evidence for Watson-Crick base pairing in vacuo. J. Am. Chem. Soc. **120**, 9605–9613 (1998)
20. Doussineau, T., Bao, C.Y., Clavier, C., Dagany, X., Kerleroux, M., Antoine, R., Dugourd, P.: Infrared multiphoton dissociation tandem charge detection-mass spectrometry of single megadalton electrosprayed ions. Rev. Sci. Instrum. **82**, 084104 (2011)
21. Doussineau, T., Antoine, R., Santacreu, M., Dugourd, P.: Pushing the limit of infrared multiphoton dissociation to megadalton-size DNA ions. J. Phys. Chem. Lett. **3**, 2141–2145 (2012)
22. Antoine, R., Doussineau, T., Dugourd, P., Calvo, F.: Multiphoton dissociation of macromolecular ions at the single-molecule level. Phys. Rev. A **87**, 013435 (2013)
23. Fuerstenau, S.D., Benner, W.H.: Molecular weight determination of megadalton DNA electrospray ions using charge detection time-of-flight mass spectrometry. Rapid Commun. Mass Spectrom. **9**, 1528–1538 (1995)
24. Schultz, J.C., Hack, C.A., Benner, W.H.: Polymerase chain reaction products analyzed by charge detection mass spectrometry. Rapid Commun. Mass Spectrom. **13**, 15–20 (1999)
25. Schultz, J.C., Hack, C.A., Benner, W.H.: Mass determination of megadalton-DNA electrospray ions using charge detection mass spectrometry. J. Am. Soc. Mass Spectrom. **9**, 305–313 (1998)
26. Cheng, X., Camp, D.G., Wu, Q., Bakhtiar, R., Springer, D.L., Morris, B.J., Bruce, J.E., Anderson, G.A., Edmonds, C.G., Smith, R.D.: Molecular weight determination of plasmid DNA using electrospray ionization mass spectrometry. Nucleic Acids Res. **24**, 2183–2189 (1996)
27. Paech, K., Jockusch, R.A., Williams, E.R.: Slow infrared laser dissociation of biomolecules in the rapid energy exchange limit (vol 106A, pg 9763, 2002). J. Phys. Chem. A **107**, 2596 (2003)
28. Bustamante, C., Bryant, Z., Smith, S.B.: Ten years of tension: single-molecule DNA mechanics. Nature **421**, 423–427 (2003)
29. Bolest, T.C., White, J.H., Cozzarelli, N.R.: Structure of plectonemically supercoiled DNA. J. Mol. Biol. **213**, 931–951 (1990)